An Experimental Study of Swirling Supercritical Hydrocarbon Fuel Jets

R. R. Rachedi

L. C. Crook

P. E. Sojka
e-mail: sojka@ecn.purdue.edu

Maurice J. Zucrow Laboratories,
School of Mechanical Engineering,
Purdue University,
West Lafayette, IN 47906-2014

An experimental investigation was conducted to examine the behavior of swirling supercritical hydrocarbon fuel (SCF) jets injected into nitrogen environments whose temperatures and pressures exceeded the fuel critical values. Measurements of jet full-cone angle, mass concentration field, and penetration length were made using a schlieren system; the images were captured by a high-speed digital camera and processed using the camera's software, plus MATLAB codes. Test parameters were the internal geometry of the pressure-swirl nozzle, fuel flow rate, and density ratio. The density ratio was varied by altering the reduced temperature of the injected fluid and nitrogen environment. SCF injections were studied at reduced temperatures (T_{jet}/T_{crit} with both reported in Kelvin) ranging between 1.01 and 1.10, a reduced pressure (p_{jet}/p_{crit} with both reported in bars) of 1.05, and fuel flowrates of 1.0 g/s, 2.0 g/s, and 3.0 g/s. The variable internal geometry pressure-swirl atomizer produced jets having swirl numbers (SN) of 0 (straight bore), 0.25, 0.50, and 1.00 (high swirl). As expected, increasing the swirl number for a SCF jet had by far the largest effect on jet cone angle, followed by a change in the density ratio; changing the fuel flow rate had very little effect. The SCF jet penetration length increased when either the fuel flow rate or density ratio increased. The mass concentration profiles demonstrated the jets to be self-similar in nature, and correlation to a Gaussian profile showed the mass concentration field to be independent of swirl number, density ratio, and fuel flow rate. Finally, it was found that there was a linear relationship between the jet half-width and the swirl number. The current study characterized the behavior of swirling hydrocarbon fuel SCF jets for the first time. Aspects of jet behavior similar to that of gas jets include: Gaussian mass concentration profiles and jet boundaries that scale with swirl number. Finally, CO_2 was found to be a suitable surrogate fluid for hydrocarbon fuels since the behavior of the hydrocarbon SCF jets was similar to that of CO_2 SCF jets. [DOI: 10.1115/1.3124668]

Keywords: supercritical injection, supercritical jets, supercritical swirling jets

1 Introduction

A supercritical fluid (SCF) is defined as one whose pressure and temperature exceed its thermodynamic critical state (i.e., critical pressure and temperature). As a fluid approaches and passes its critical point, its properties vary substantially. For example, it experiences large variations in density and loses surface tension. These property variations can have profound effects on the behavior of swirling jets.

Interest in SCF jets has arisen because of recent developments in the gas turbine industry, which have created a demand for engines capable of propelling aircraft at speeds exceeding Mach 4, with future expectations of speeds reaching Mach 7. At these speeds the heat produced by friction on the air frame, higher pressure-ratio engine components, and additional electronics is expected to be large enough that the current method of cooling (using ambient air) will no longer be adequate. As a result, an additional heat sink is being sought.

One proposed solution is to use the aircraft's onboard fuel as the additional heat sink. In this scenario, the fuel would be routed through the airframe and engine prior to injection into the combustion chamber.

There is a consequence of using a fuel-based heat sink—the energy removed could be enough to heat the fuel beyond its critical temperature. Combined with the fact that fuel pressures within gas turbine engines already exceed their critical value, the fuel would be in a supercritical state prior to injection.

The existence of SCF at the point of injection obviously requires a thorough understanding of how supercritical jets behave. Without this information, the supercritical threshold would be the limit for a fuel heat sink design. Obtaining such an understanding is the motivation for this research, thereby enabling injector designs capable of supplying fuels that are in the supercritical state.

A review of the current literature shows several studies [1–3] have found that SCF jets injected into supercritical environments exhibit behavior similar to that of gas jets. Not surprisingly, it was found that the similarity between SCF and gas jet behavior increased as the thermodynamic state of the SCF jet moved further past the critical point. The literature also suggests that as a jet's temperature or pressure increases to values much greater than the critical point, the jet's density ratio become increasingly similar to the ratios found in gas jets.

The aim of the current study was to extend recent SCF jet experiments [2] from CO_2 to hydrocarbon based jet fuels. In particular, we sought to determine if CO_2 behavior and scalings already reported are applicable to typical aircraft fuels.

Three characteristics were identified as being important to SCF jet processes: (1) jet cone angle, (2) fuel mass concentration field, and (3) penetration length. Changes in these characteristics were examined as the density ratio between the fuel and environment, fuel flow rate, and injector internal geometry of the pressure-swirl nozzle were varied. In particular, experiments were conducted using JP-10 at a reduced pressure (p_{jet}/p_{crit} with both reported in

Manuscript received July 24, 2007; final manuscript received April 8, 2008; published online May 18, 2010. Review conducted by Nader Rizk. Paper presented at the 2007 ASME International Mechanical Engineering Congress (IMECE2007), Seattle, WA, November 10–16, 2007.

Table 1 Critical properties of selected fuels

Fuel	K	MPa
JP-10	698	3.73
JP-8P	656	2.45
Jet-A	671	2.38

bars) of 1.05, reduced temperatures (T_{jet}/T_{crit} with both reported in Kelvin) between 1.01 and 1.10, and fuel flow rates of 1–3 g/s.

JP-10 was chosen mostly because it is a single-component fuel, an attribute that makes interpretation of refractive index measurements straightforward, but also because its critical temperature is within about 5% of those for JP-8 and Jet-A (two more widely used fuels). The only disadvantage of using JP-10 is that its critical pressure is about 35% higher than those for JP-8 and Jet-A (Table 1).

The Reynolds numbers of the SCF jets in the current experiment were similar to those of a turbulent gas jet and ranged between 70,000 and 180,000. The injections occurred in supercritical nitrogen environments that were at reduced temperatures matching the fuel temperature and reduced pressures of 1.05. Injection was accomplished using a pressure-swirl atomizer having a variable internal geometry. Jets were described by swirl numbers (*SN*), where the swirl number is the ratio of the initial angular momentum flux to the initial axial momentum flux, with values of 0 (straight bore), 0.25, 0.50, and 1.00.

Measurements of the jet cone angle, mass concentration field, and penetration length were made using a schlieren system. Images produced by the schlieren system were captured by a high-speed camera and processed with the use of the high-speed camera's software and MATLAB codes.

In summary, the current study simulated conditions within a gas turbine engine where SCF injection would occur. It represents the first study of the behavior of swirling supercritical hydrocarbon-based fuels injected into environments whose temperature and pressure exceeded the fuels' critical values. The data from these experiments serve two purposes. It allows the mechanisms, which control the physical behavior of the SCF jets to be identified, and may help relate the behavior of SCF jets to other supercritical jets such as CO_2. The behavioral characteristics could then be used to design injectors, which can optimally inject SCF fuels into gas turbine engines.

2 Experimental Apparatus

The SCF experiments were conducted in a newly constructed high-pressure/high-temperature facility at the Rolls-Royce University Technology Center for High-Mach Propulsion, part of the Maurice Zucrow Laboratories at Purdue University. The experimental setup is composed of the test vessel, nitrogen coflow system, fuel supply system, data acquisition system, pressure-swirl nozzle, and schlieren optical system.

The pressure vessel contains the N_2-filled environment whose temperature and pressure exceed the critical point of JP-10. It is capable of withstanding 4.14 MPa at 650°C. A honeycomb flow straightener inside the vessel is used to ensure the nitrogen coflow closely approximates a 1D flow field.

The vessel has four points of optical access. Two of them (6.35 cm diameter clear aperture) are diametrically opposite each other and are used with the schlieren system. The remaining two are for PDA measurements (which were not made during this study).

Operating conditions were measured at several locations throughout the vessel using Omega type-K thermocouples and Druck PMP-1260 pressure transducers. To minimize temperature gradients inside the vessel, the temperature was monitored at the vessel wall parallel to the injection section, at the injection point, and at a distance 7 cm downstream of the injection point.

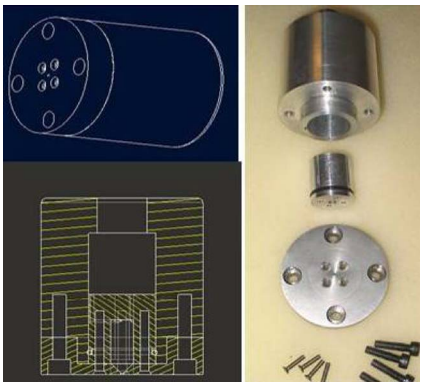

Fig. 1 Pressure-swirl nozzle

A N_2 coflow system provides a heated inert environment where fuel injection can occur without the dangers of combustion. The heating unit supplies a 1D flow at temperatures as high as 650°C (1200°F). After exiting the heater, the N_2 temperature can be maintained, or raised, prior to entering the pressure vessel by three sets of rope heaters. Previous studies [4] have shown that removal of dissolved O_2 from jet fuel can significantly reduce the amount of coking the fuel will experience as it is heated, so a sparging system was included.

A pressure-swirl nozzle was used as the fuel injector, see Fig. 1. It is identical in design to the one used by Zeaton [2], except for modifications made to allow for operation in high-temperature environments.

Similar to Zeaton [2], SCF jets produced from four different pressure-swirl nozzle configurations were used in this study. The jets were classified by their swirl numbers (*SN*) [5]

$$SN = \frac{\pi d_o^2}{4A_p} \tag{1}$$

where d_o is the exit orifice diameter and A_p is the total area of the inlet ports. Using the expression of Syred et al. [5] and the Beer–Chigier [6] definition of swirl magnitude, the current experiment studied jets with swirl numbers of 0.0 (straight bore, no swirl), 0.25 (low swirl), 0.50 (moderate swirl), and 1.00 (high swirl).

The schlieren optical system used for capturing images of SCF jet evolution is shown in Fig. 2(*a*). It is identical to the setup used by Zeaton [2], and was originally designed by Settles [7], with the exception that the current setup uses a horizontal z-type configuration as opposed to the vertical z-type configuration of Zeaton.

Light from a light source (Altman 6X22 ellipsoidal theater stage light with a 1000W FEL-type lamp) was focused using an aspheric condenser lens and directed onto the end of a fiber-optic cable. A rectangular slit was placed at the output end of the fiber-optic cable to create a quasi-uniform light source. Light from the fiber-optic is then reflected off a slightly tilted (~3 deg) 108 mm diameter, f/6 parabolic mirror before passing through the test section (injection point inside the pressure vessel). Upon exiting the test section, the light is reflected off an identical, but oppositely angled, f/6 mirror. The identical opposition in angles between the two mirrors offsets any comatic aberrations, which may occur due to the original mirror angle.

After reflection off the second mirror, the light is reflected one last time off a plane mirror. The reflected light then passes by the knife edge, which is set to cut off 50% of the light. The percent cutoff of the knife edge was set by an adjustable microdrive linear translation mount, which is accurate to ±0.01 mm. The knife edge was vertically oriented to measure cone angle, mass concentration fields, and jet penetration length.

To ensure that the image aberrations were kept to a minimum, a transparent square grid pattern was placed in the light beam path,

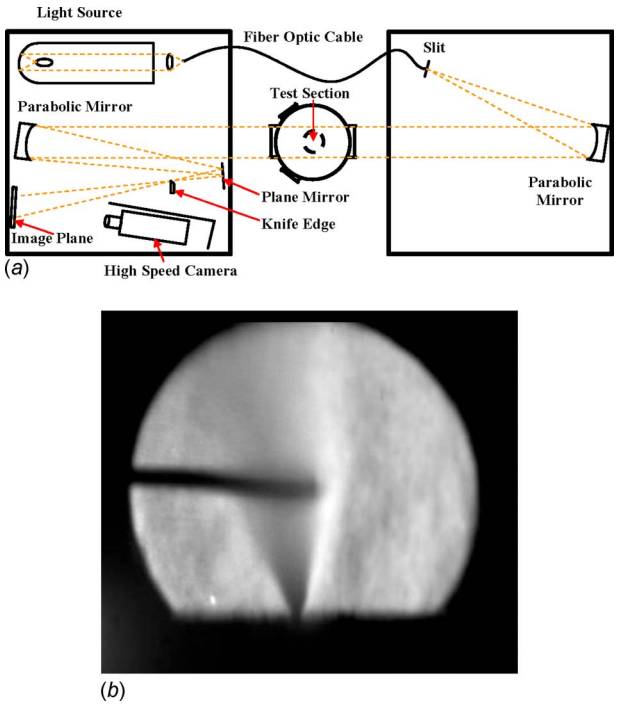

Fig. 2 (*a*) Schlieren system and (*b*) typical schlieren image (averaged over 1 s) captured using the system shown in (*a*)

as recommended by Settles [7]. The parabolic mirror angles were adjusted until negligible barrel or pincushion distortion was observed.

After passing the knife edge, the light produces a real inverted image on the image plane. A high-speed camera (Vision Research Phantom v5.1 capable of capturing 1024×1024 monochrome images at framing rates up to 1200 Hz) records jet behavior at a rate of 100 images per second. Image bursts are typically 2–5 s during experiments, well within the camera's on-board storage capacity of >29 s. The images are viewed as individual pictures, or together as a video. When viewed as individual pictures, no evidence of critical opalescence (the "cloudiness" reported by numerous authors that is due to spatial density fluctuations whose magnitude is near or larger than the wavelength of light) was observed.

When computing concentration fields for jet cone angle and penetration length the entire image burst is used giving 200–500 images for each data point. A typical schlieren image (but averaged for only 1 s) is presented, as shown in Fig. 2(*b*).

Concentration data are extracted from the schlieren pixel intensity values by analyzing images using Keagy and Ellis' [8] approach and a Schardin transformation. The Schardin transformation assumes the jet to have axisymmetric inhomogeneities such that it can be divided into a number of small rings (m), where the index of refraction is constant in each ring. In this study, the width of a pixel ($\sim$0.17 mm) was assumed to be a suitable width for each ring.

The first step is to calculate the refractive index gradient for the outermost ring (jet edge) by using image contrast and

$$\frac{\Delta I}{I} = \frac{\Delta a}{a} = \frac{f\alpha}{a} \tag{2}$$

where α is the angle at which a schlieren beam is deflected.

The next step is to move inward to the second ring and to calculate its index of refraction gradient. This newly calculated gradient is the sum of the gradients from the first and second rings, so the gradient of the second ring can be found when the gradient of the first ring is subtracted from the sum.

This process is repeated for every ring until the centerline of the jet is reached. After the refractive index gradient for every ring has been calculated, the index of refraction at each ring i is determined by direct summation

$$n_i = n_0 + \sum_{j=1}^{i} \left(\frac{\partial n}{\partial r}\right)\frac{R}{m} \tag{3}$$

where n_i is the refractive index at ring i, and

$$\left(\frac{\partial n}{\partial r}\right)_i = \frac{n_0 \varepsilon_{yi}}{R}\frac{1}{2}\left[\frac{m-i}{m}\cosh^{-1}\left(\frac{m+1-i}{m-i}\right)\right]^{-1} - \sum_i \tag{4}$$

$$\sum_i = \left[\cosh^{-1}\left(\frac{m+1-i}{m-i}\right)\right]^{-1}\sum_{j=1}^{i-1}\left(\frac{\partial n}{\partial r}\right) \times \left[\cosh^{-1}\left(\frac{m+1-j}{m-i}\right) - \cosh\left(\frac{m-j}{m-i}\right)\right] \tag{5}$$

Here R is the total radius of the jet at a particular axial location (i.e., $x/d_o = 10, 20, 40$).

Since the mixture index of refraction at each ring can be found by Eq. (3), and the index of refraction of pure JP-10 ($n_{\text{JP-10}}$) and pure nitrogen (n_{N_2}) are known quantities, Eq. (6) can be used to find the concentration of JP-10 at each location in the jet

$$\varphi_1 = \left(\frac{n_i - n_{N_2}}{n_{\text{JP-10}} - n_{N_2}}\right) \tag{6}$$

Jet cone full-angle was calculated by measuring the distance between the visual jet boundary and the centerline of the jet (y) at a given axial distance from the center of the atomizer exit orifice (x), and determining the angle formed via geometry, then doubling it. This definition is similar to that of Dodge and Biaglow [9] and Jang et al. [10], and was chosen for its simplicity. To evaluate experimental uncertainty and to minimize the influence of single operator bias, multiple observers independently marked the visual edge of each jet, with the uncertainty then calculated from the variance in the edge locations.

Kline and McClintock's [11] method for calculating the propagation of measurement uncertainties was used to determine the uncertainties in the cone angle, penetration length and mass concentration field data. Typical uncertainties are 5%, 11%, and 10%, respectively.

3 Results

Data were collected for jets with $SN = 0.25$, 0.50, and 1.00. Cone half-angles were measured from schlieren images at axial locations of $x/d_o = 10$, 20, and 40, where x is the axial distance from the orifice, and d_o is the atomizer exit orifice diameter (1 mm). Jet reduced pressure was 1.05, density ratios ranged from $\rho_{\text{JP-10}}/\rho_{N_2} = 6$ to 10, and fuel flowrates were 1 g/s, 2 g/s, and 3 g/s. The density ratio was varied by increasing the temperature of the test fuel and nitrogen environment.

Figures 3–6 show measured full-cone angles as a function of density ratio produced by the $SN = 0$, 0.25, 0.50, and 1.00 nozzles at three different axial locations downstream of the injection point. It is clear that jet cone angle decreases at axial locations further downstream from the injection point for all swirl nozzles with nonzero SN. The cone-angle collapse is attributed to N_2 being entrained into the jet. The $SN = 0$ jet results can be explained by behavior noted by Guildenbecher et al. [12] and Ortman and Lefebvre [13], who both stated that there exists a threshold where the cone angle of a jet is so small that the effects of entrainment can no longer cause the cone angle to noticeably contract. In the case of the $SN = 0$ jet, the full-cone angle is significantly smaller

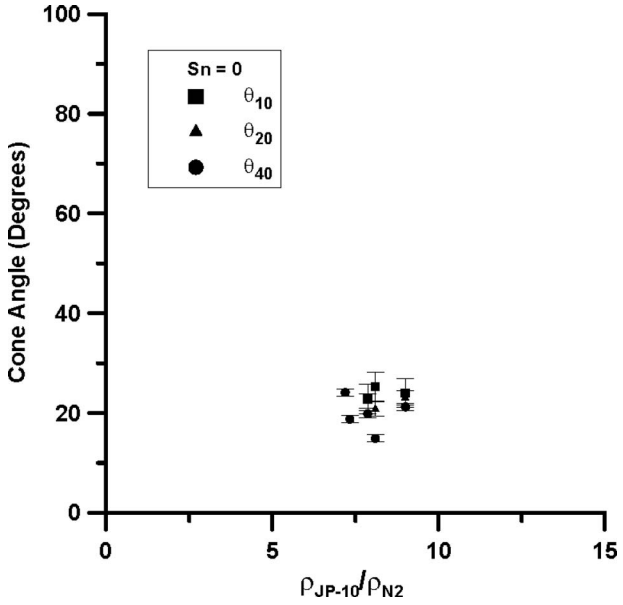

Fig. 3 Full-cone angle versus density ratio for *SN*=0.0

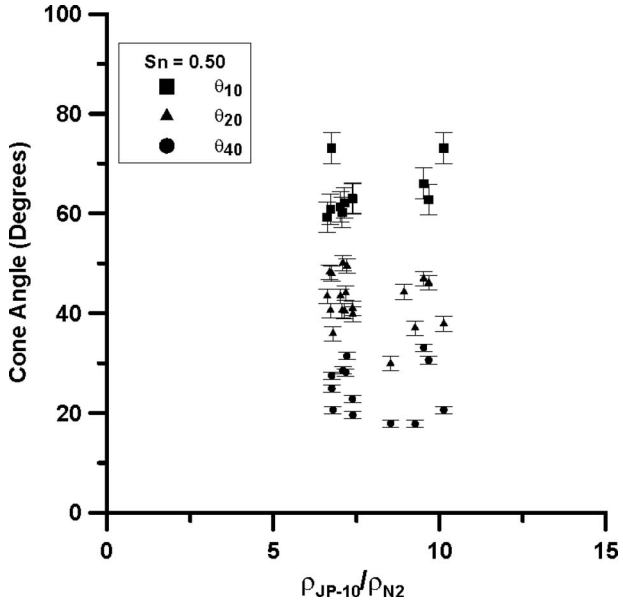

Fig. 5 Full-cone angle versus density ratio for *SN*=0.50

than full-cone angles for the higher swirl jets and appears to be small enough that the entrainment of the surrounding nitrogen cannot be observed.

Figure 7 presents θ_{20} versus density ratio for a fuel flow rate of 1 g/s. It shows the expected behavior that increasing *SN* causes the jet full-cone angle to increase. This behavior was observed for all fuel flow rates. The increase in full-cone angle as *SN* increases is not a surprising result; nozzles with larger swirl numbers induce larger amounts of angular momentum, which cause the fluid to spread in the radial direction at a faster rate. Zeaton [2] saw the same behavior in his supercritical CO_2 injections, thus the influence of internal geometry on the cone angle for fuel jets is analogous to that for SCF CO_2 jets.

Figure 8 presents θ_{10} versus density ratio as fuel flow rate is varied. While there is a slight dependence of θ_{10} on density ratio, when considering the experimental uncertainty in determining θ_{10}, the conclusion is that changing density ratio does not have a significant effect on jet full-cone angle. This result is similar to the findings of Zeaton [2] and was consistent across all swirl nozzle geometries tested.

Figures 9 and 10 show θ_{20} versus density ratio as the fuel flow rate is varied for jets with swirl numbers of 0.25 and 0.50. Note that increasing fuel flow rate has no noticeable effect on jet full-cone angle. Zeaton [2] reported the same behavior in his SCF CO_2 study

In summary, the following results of the cone-angle portion of this study are very similar to those of Zeaton's [2] supercritical CO_2 study.

- Changing *SN* has by far the largest effect on jet full-cone angle, with higher swirl numbers producing larger cone angles (as expected).
- Changing density ratio had the next largest impact on full-

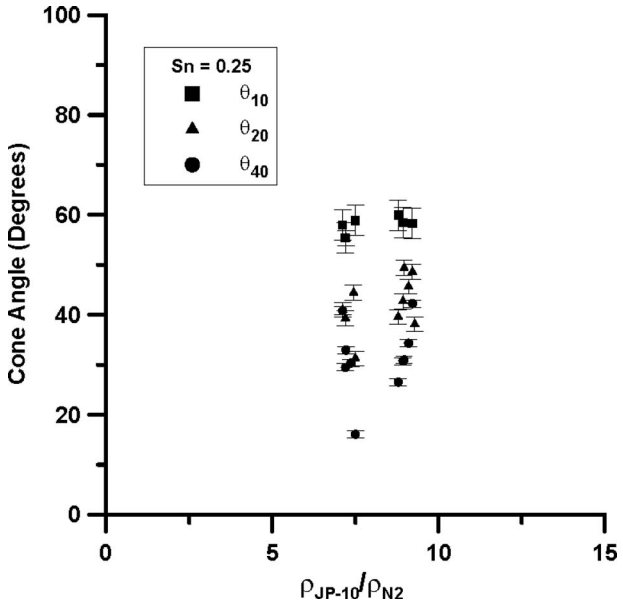

Fig. 4 Full-cone angle versus density ratio for *SN*=0.25

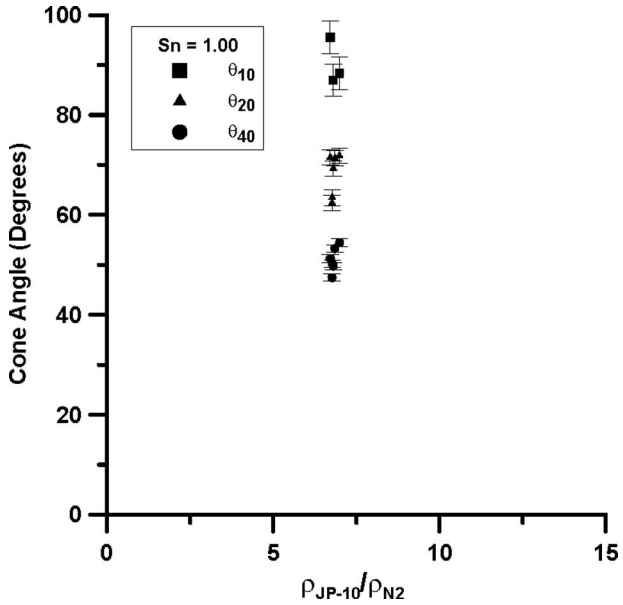

Fig. 6 Full-cone angle versus density ratio for *SN*=1.00

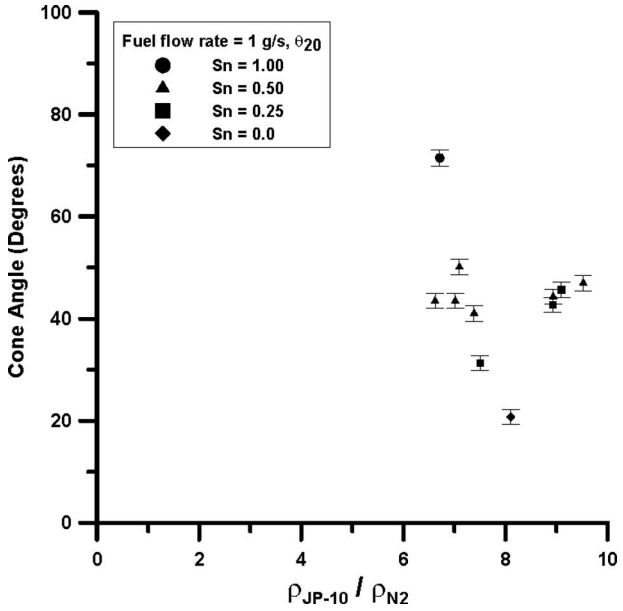

Fig. 7 θ_{20} versus density ratio for a fuel flow rate of 1.0 g/s

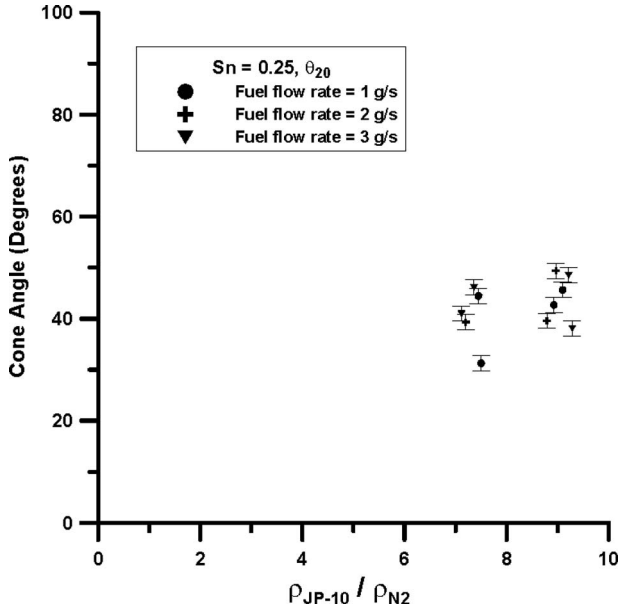

Fig. 9 θ_{20} versus density ratio as fuel flow rate varies for *SN* =0.25

cone angle, with an increase in density ratio yielding a slight increase in cone angle.

- Changing fuel flow rate has no significant effect on jet full-cone angle.
- The full-cone angle for all the SCF jets with swirl numbers not equal to 0 collapsed as the jet propagated downstream from the injector due to entrainment of the surrounding environment
- The full-cone angle for the $SN=0$ jet was so small that the effects of entrainment could not cause the jet cone angle to collapse as it propagated downstream from the injector.

Recall that Keagy and Ellis' approach [8] and a Schardin transformation were used to extract fuel mass concentration profiles from the schlieren pixel intensity maps. Figures 11–14 show the mass concentration profiles for the jets with swirl numbers of 0, 0.25, 0.50, and 1.00 measured at an axial distance of $x/d_o=60$. It should be noted that these plots are representative of each axial location ($x/d_o=20$, 40, 60, and 70) and all swirl numbers tested. The vertical axis in the plots is the jet mole fraction (Y) normalized by its centerline value (Y_{cl}), the horizontal axis is the jet radial location normalized by the jet half-radius ($r_{0.5}$), where the jet half-radius is the location where the fuel concentration decays to half its centerline value.

A comparison of Figs. 11–14 shows concentration data plotted using nondimensionalization by the jet half-radius collapse onto nearly identical curves. This behavior was also observed by Zeaton [2] in his study of supercritical CO_2 jets, and suggests that the SCF JP-10 jets are self-similar.

The effects of increasing density ratio on the mass distribution field are also shown in Figs. 11–14; however, Figs. 12 and 13, which represent $SN=0.25$ and $SN=0.50$, show the largest varia-

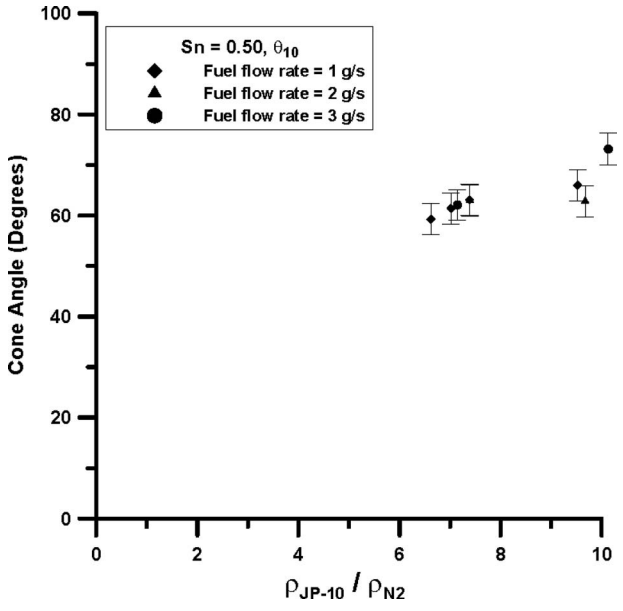

Fig. 8 θ_{10} versus density ratio for *SN*=0.5

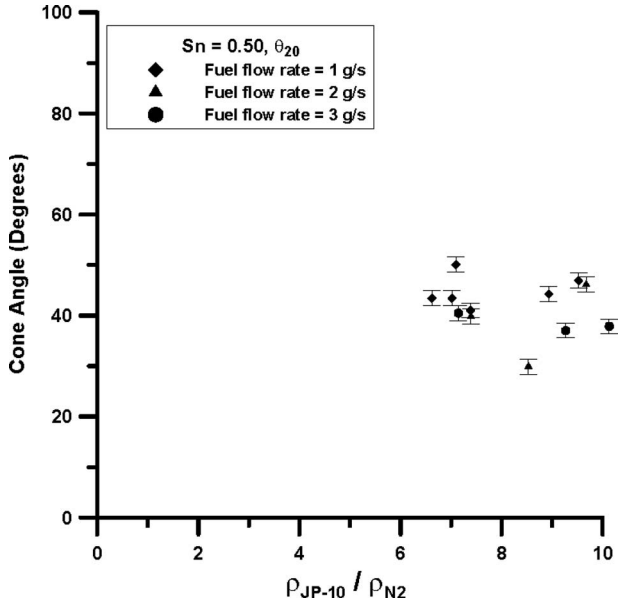

Fig. 10 θ_{20} versus density ratio as fuel flow rate varies for *SN*=0.50

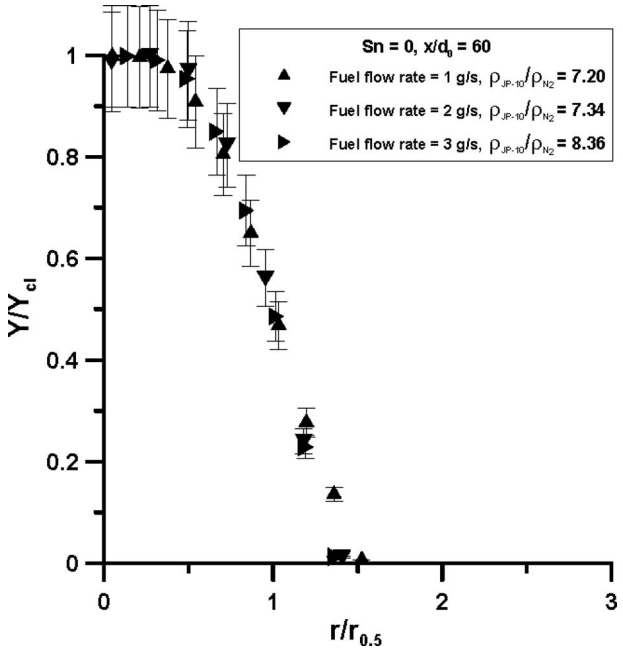

Fig. 11 Fuel mass distribution versus jet radial location normalized by the jet half-radius, *SN*=0 and x/d_o=60

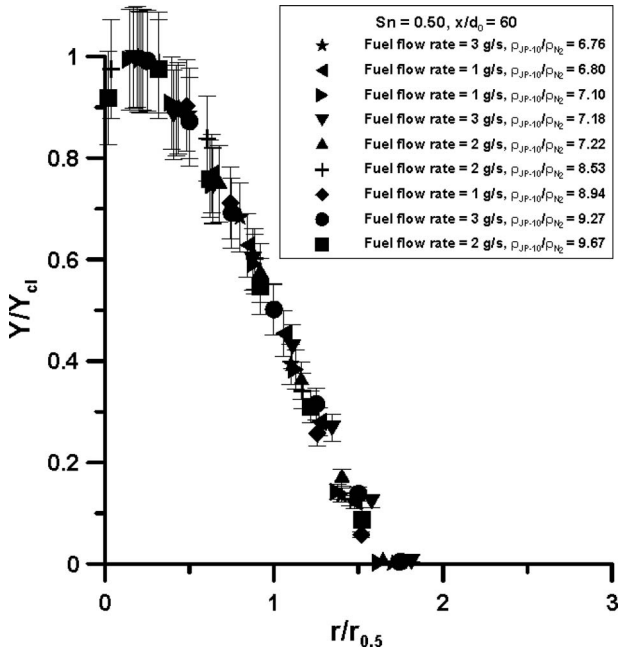

Fig. 13 Fuel mass distribution versus jet radial location normalized by the jet half-radius, *SN*=0.50 and x/d_o=60

tions in density ratios. Upon examining figures for the *SN*=0.25 and *SN*=0.50 nozzles, the curves for each axial location appear to be similar to one another, leading to the conclusion that increasing density ratio has a minimal effect on jet mass distribution field. This behavior is also seen for the *SN*=0 and *SN*=1.00 data.

The effect of fuel flow rate on the mass concentration field can also be seen in Figs. 11–14. It can be observed from the figures that, just as with cone angle, increasing the fuel flow rate has no distinguishable effect on the mass concentration field. This behavior was observed by Zeaton [2] in his supercritical CO_2 study. It has been theorized that the momentum transfer in SCF jets behaves similarly to the turbulent diffusivity for mass transfer in free turbulent gas jets, thus the concentration decay in a SCF jet would be analogous to the velocity decay in a free turbulent gas jet. In this scenario the velocity decay is independent of the Reynolds number [14], and thus the concentration profile would be independent of the fuel flow rate.

The effect of atomizer internal geometry on the mass concentration field of SCF jets is presented next. The effects of internal geometry can be seen by consideration of the mass concentration plots displayed thus far. An examination of the plots suggests that

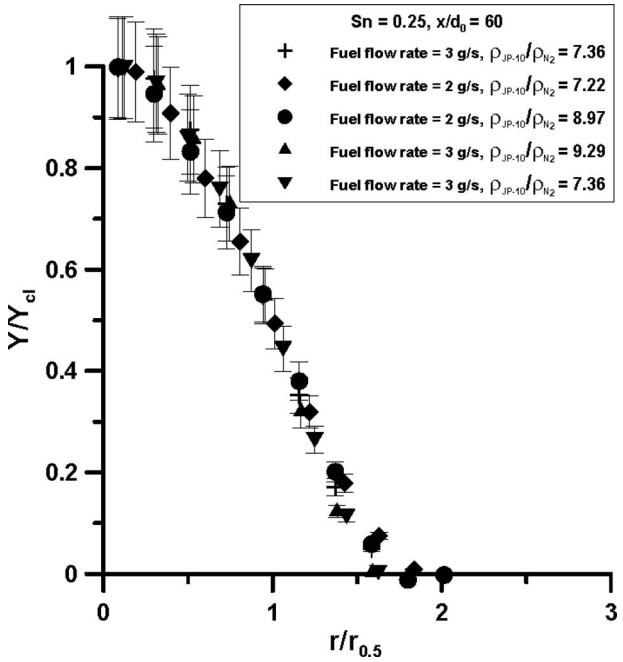

Fig. 12 Fuel mass distribution versus jet radial location normalized by the jet half-radius, *SN*=0.25 and x/d_o=60

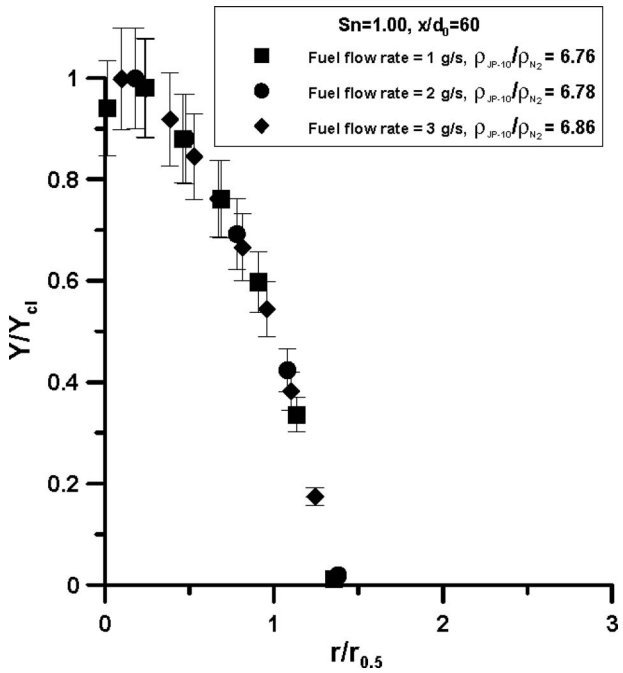

Fig. 14 Fuel mass distribution versus jet radial location normalized by the jet half-radius, *SN*=1.00 and x/d_o=60

Table 2 Spreading parameters, σ, for SCF jets

	σ			
x/d_o	20	40	60	70
SN				
0	0.65	0.68	0.64	0.63
0.25	0.60	0.60	0.63	0.62
0.5	0.61	0.65	0.64	0.64
1	0.67	0.63	0.61	0.62

the swirl number of the nozzle does not have an effect on mass concentration profile. However, to confirm this result, a quantitative measurement was sought.

To accomplish this, the SCF jet mass distribution data were fit to a Gaussian profile

$$Y/Y_{CL} = e^{-(r/r_{0.5})^2/2\sigma} \quad (7)$$

Results for $SN=0$, 0.25, 0.50, and 1.00 were used. Values for the spreading parameter, σ, were calculated at axial distances of $x/d_o=20$, 40, 60, and 70. Table 2 shows the results at each corresponding axial location. The mean of the spreading parameters is 0.63 and the standard deviation is 0.02. Since 14 out of the 16 σ values fall within one standard deviation of the mean, and all points are within two standard deviations, it can be concluded that that the spreading parameter is independent of axial location (x/d_o), swirl number, density ratio, and fuel flow rate and is only dependent on the jet half-width.

Next, the jet half-width was examined to determine whether a correlation could be found to relate it either to the axial distance downstream from the injector, or to the injector swirl number. Jet half-widths at axial locations of $x/d_o=20$, 40, 60, and 70 are shown in Table 3. No correlation could be found between jet half-width and the axial distance downstream from the injector. This is attributed to the effects of entrainment, which cause the cone angles to collapse.

When examining jet half-width versus *SN* at a specific axial location, the jet half-width is seen to increase with *SN*. This result is expected because pressure-swirl nozzles with higher swirl numbers create jets with larger cone angles. Jets with larger cone angles have wider dispersions of fuel so the jet half-width should occur at radial locations further from the jet centerline.

Since jet half-width appeared to have a linear relationship with *SN*, correlations were attempted for axial distances of $x/d_o=20$, 40, 60, and 70. They are of the form $r_{0.5}=M*SN+B$, and are shown in Table 4.

The penetration length of SCF jets as the fuel flow rate and density ratios were varied is now presented. For the purposes of this study, the jet penetration length is defined to be the distance downstream from the injector where the centerline fuel concentration had decayed to 20% of the centerline fuel concentration at an axial distance of $x/d_o=20$. This definition was chosen for two reasons. First, accurate measurements of centerline fuel concentration could not be made closer than $x/d_o=20$ from the atomizer exit plane. Second, fuel centerline concentration data became noisy for values below 20% of the $x/d_o=20$ value. The method

Table 3 Jet half-width ($r/r_{0.5}$)

	SN			
x/d_o	0	0.25	0.50	1.00
20	7.06	11.18	11.31	13.17
40	7.62	11.01	11.63	14.76
60	9.14	11.35	11.80	16.40
70	10.10	10.84	11.64	18.07

Table 4 Linear correlation of jet half-width to swirl number

x/d_o	$M*SN$	B	R^2
20	$5.36*SN$	8.34	0.79
40	$6.64*SN$	8.35	0.97
60	$7.02*SN$	9.10	0.98
70	$8.12*SN$	9.11	0.90

for determining the centerline fuel concentration was the same as that used for determining the mass concentration field.

Figures 15–17 show the effect of increasing fuel flow rate from 1 g/s to 3 g/s for the $SN=0.50$ jet at several density ratios. The literature [1], as well as physical arguments, suggests that increas-

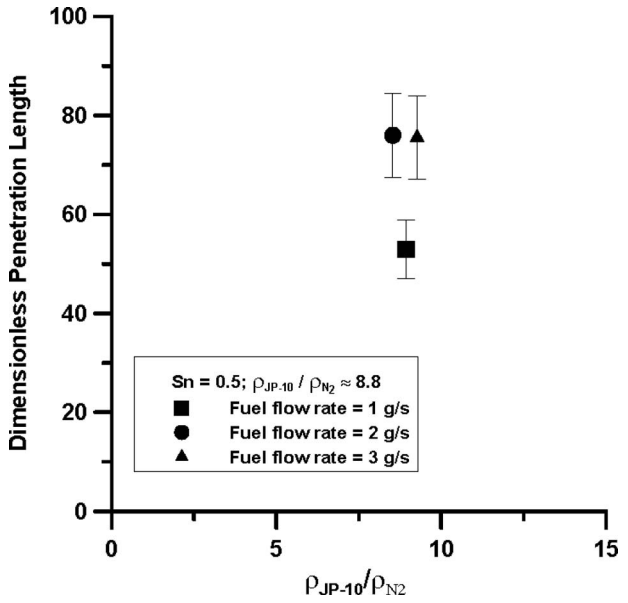

Fig. 15 Penetration length versus axial position, $SN=0.5$, $\rho_{JP\text{-}10}/\rho_{N_2} \approx 8.8$

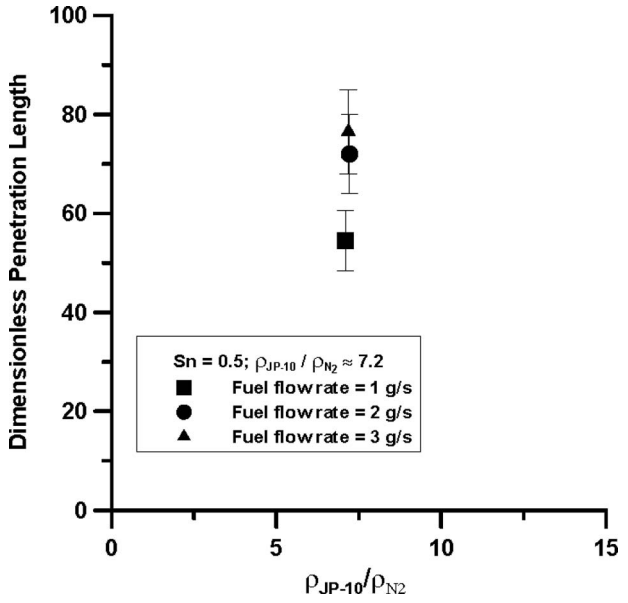

Fig. 16 Penetration length versus axial position, $SN=0.5$, $\rho_{JP\text{-}10}/\rho_{N_2} \approx 7.2$

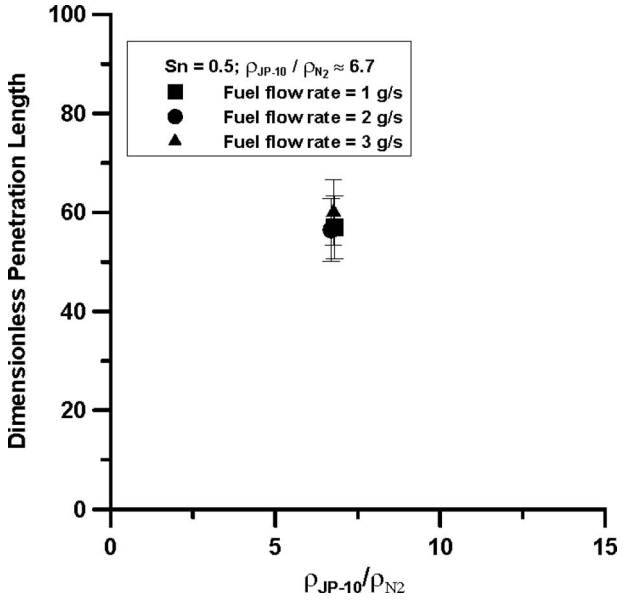

Fig. 17 Penetration length versus axial position, $SN=0.5$, $\rho_{JP\text{-}10}/\rho_{N_2} \approx 6.7$

ing the fuel flow rate will increase jet penetration length. This is the case for the SCF JP-10 injections studied here.

Another interesting observation is that the effect of increasing fuel rate depends on the magnitude of the density ratio. In Figs. 15–17 the difference in penetration length between the jets with fuel flow rates of 1 g/s and 3 g/s decreases as the density ratio decreases from an approximate value of 8.8 to a value of 6.7. This phenomenon was observed in both nozzles tested. This behavior is ascribed to an increase in mixing between the SCF jet and surrounding environment as the density ratio decreases. This leads to enhanced jet dissipation, which eventually dominates the effects of increasing fuel flow rate.

The last aspect considered was the effect of density ratio on penetration length. Density ratio was varied by increasing the temperature of both the fuel and surrounding nitrogen. The literature [2,15] states that denser jets have higher initial inertia and this higher initial inertia should cause the jets to penetrate farther upon injection. In fact, this behavior can be seen in Figs. 15–17.

It was stated earlier that the effect of fuel flow rate was coupled with the density ratio. The effect of the fuel flow rate on penetration length diminished as the density ratio decreased, and it was reasoned that this behavior occurred because mixing of the fuel and surrounding nitrogen, which reduces the penetration length, became more important due to the decrease in density. This explanation is supported by data presented in this section, which demonstrates that decreasing the density ratio decreased the jet's inertia, thereby make mixing effects more significant and resulting in jets with shorter penetration lengths.

4 Summary and Conclusions

Cone angles, penetration lengths, and concentration fields for supercritical fluid jets of JP-10 were measured using high-speed schlieren photography. Jets were formed using atomizers with swirl numbers of 0.0, 0.25, 0.50, and 1.00. Fuel flow rate was varied between 1 g/s, 2 g/s, and 3 g/s. The following conclusions can be drawn from the data.

- Increasing the swirl number for a SCF fluid has the largest effect on jet cone angle, followed by a change in the density ratio; changing the fuel flow rate had almost no effect.
- Cone angle increases as the jet swirl number increases. The increase in cone angle is due to the additional angular momentum imparted on the injected fluid.
- Cone angle slightly increases as the density ratio between the injected fluid (JP-10) and the environment (nitrogen) increases. This is due to an increase in angular momentum as the fluid density increases.
- The cone angle of an SCF jet decreases at axial distances further downstream from the injection point. Entrainment of the surrounding nitrogen causes the jet to collapse.
- The SCF jets were self-similar in nature. The mass concentration profile was found to be independent of swirl number, fuel flow rate, and density ratio.
- The jet half-width has a linear relationship with the swirl number of the jet.
- Increases in fuel flow rate caused the penetration length to increase, but the magnitude of the increase is coupled to the density ratio. It is believed that mixing between the SCF fuel and the environment, which causes the jet to dissipate and shortens the penetration length, begins to dominate the effects of increasing the jet fuel flow rate as the density ratio decreases.
- SCF jet penetration length decreases as the density ratio decreases. The decrease in density ratio makes the jet more susceptible to mixing effects, which occurs between the jet and the surrounding nitrogen. This mixing dissipates the jet energy and causes the penetration length to decrease.

A comparison between the behaviors of a hydrocarbon SCF jet and a CO_2 SCF jet found their behaviors to be similar in most regards: changing the jet swirl number was the most effective way of modifying cone angle, while changing density ratio had a minor effect; increasing density ratio increased jet penetration length. The only observed difference was that varying the CO_2 flow rate had no effect on penetration length, while increasing fuel flow rate caused an increase in penetration length of the hydrocarbon jets with the magnitude of that effect related to the density ratio. The difference in density ratio ranges may explain why changing fuel flow rate was found to have two different effects on penetration length. Finally, comparison of CO_2 and hydrocarbon SCF jet mass concentration field showed they both appeared to be self-similar in nature. As a result, future experiments for which the study of hydrocarbon SCF jets is desired can be performed using CO_2 as a surrogate fluid, within the range of density ratio agreement between the two fluids.

Acknowledgment

The authors would like to thank the Rolls-Royce University Technology Center for High Mach Propulsion for making this project possible. LCC also thanks the National Science Foundation for supporting him through a Graduate Research Fellowship.

Nomenclature

Symbols

A_p = total area of inlet ports (m^2)
B = intercept in the expression relating jet half-radius and swirl number (m)
d_o = nozzle exit orifice diameter (m)
M = slope in the expression relating jet half-radius and swirl number (m)
SN = swirl number (dimensionless)
r = radial location (m)
$r_{0.5}$ = jet half-radius (m)
x = distance downstream of injector exit plane, m
y = radial distance from jet centerline m
Y = jet concentration value
Y_{cl} = jet centerline concentration value
θ_{10} = cone angle measured at $x/d_o=10$ (deg)

θ_{20} = cone angle measured at $x/d_o=20$ (deg)
θ_{40} = cone angle measured at $x/d_o=40$ (deg)
θ_{HCA} = half cone angle (deg)
$\rho_{JP\text{-}10}$ = SCF density (kg/m^3)
ρ_{N_2} = ambient gas density (kg/m^3)
σ = spreading parameter (dimensionless)

References

[1] Doungthip, T., Ervin, J., Williams, T., and Bento, J., 2002, "Studies of Injection of Jet Fuel at Supercritical Conditions," Ind. Eng. Chem. Res., **41**, pp. 5856–5866.
[2] Zeaton, G., 2004, "An Experimental Study of Supercritical Fluid Jets," MS thesis, Purdue University, West Lafayette, IN.
[3] Wu, P. K., and Chen, T. H., 1996, "Injection of Supercritical Ethylene in Nitrogen," J. Propul. Power, **12**(4), pp. 770–777.
[4] Briggs, E., 2005, "Comparative Study of Prolytic Coking of JP-8 and JP-10 on Inconnel and Stainless Steel Surfaces," MS thesis, Purdue University, West Lafayette, IN.
[5] Syred, N., Gupta, A. K., and Beer, J. M., 1954, "Temperature and Density Gradient Changes Arising With the Precessing Vortex Core and Vortex Breakdown in Swirl Burners," Fifteenth Symposium (International) on Combustion, pp. 587–597.
[6] Beer, J. M., and Chigier, N. A., 1972, *Combustion Aerodynamics*, Wiley, New York.
[7] Settles, G. S., 2001, *Schlieren and Shadowgraph Techniques*, Springer, New York.
[8] Keagy, W. R., and Ellis, H. H., 1949, "The Application of the Schlieren Method to the Quantitative Measurement of Mixing Gases in Jets," Third Symposium on Combustion and Flame and Explosion Phenomena, pp. 667–674.
[9] Dodge, L. G., and Biaglow, J. A., 1986, "Effect of Elevated Temperature and Pressure on Sprays From Simplex Swirl Atomizers," ASME J. Eng. Gas Turbines Power, **108**, pp. 209–215.
[10] Jang, C., Bae, C., and Choi, C., 2000, "Characterization of Prototype High-Pressure Swirl Injector Nozzles, Part I: Prototype Development and Initial Characterization of Sprays," Atomization Sprays, **10**, pp. 159–178.
[11] Kline, S. J., and McClintock, F. A., 1953, "Describing Uncertainties in Single-Sample Experiments," Mech. Eng., **75**, pp. 3–9.
[12] Guildenbecher, D. R., Rachedi, R. R., and Sojka, P. E., 2006, "Pressure Scaling of Pressure Swirl Atomizers," *Proceedings of IMECE2006: 2006 ASME International Mechanical Engineering Congress and Exposition*, Nov. 11–15.
[13] Ortman, J., and Lefebvre, A. H., 1985, "Fuel Distributions From Pressure-Swirl Atomizers," AIAA J., **1**(1), pp. 11–15.
[14] Turns, S. R., 1996, *An Introduction to Combustion*, McGraw-Hill, New York.
[15] Chen, L., 1994, "Heat Transfer, Fouling, and Combustion of Supercritical Fuels," Defense Technical Information Center, Technical Report No. 940321.